Efficient *p-i-n* type organic solar cells incorporating 1,4,5,8-naphthalenetetracarboxylic dianhydride as transparent electron transport material

Christiane Falkenberg,[a] Christian Uhrich,[b] Selina Olthof, Bert Maennig,[b] Moritz K. Riede, and Karl Leo[c]
Institut für Angewandte Photophysik, Technische Universität Dresden, D-01069 Dresden, Germany

(Received 13 March 2008; accepted 31 May 2008; published online 6 August 2008)

The implementation of proper charge carrier transport materials in *p-i-n* type organic solar cells strongly influences the device performance. Our investigation focuses on the substitution of the standard layer sequence used at the side of electron transport, usually consisting of either C_{60}/exciton blocking layer/metal or *n*-C_{60}/metal by a layer sequence including a window layer. Here, we evaluate the transparent electron transport material 1,4,5,8-naphthalenetetracarboxylic dianhydride (NTCDA), which guarantees a loss free charge extraction from the active materials due to a good energy level alignment as well as exciton blocking due to its wide bandgap. It is demonstrated that upon the exchange of the electron transport layer *n*-C_{60} for *n*-NTCDA, the solar power conversion efficiency of a *p-i-n* device can be increased by 10%. © *2008 American Institute of Physics*. [DOI: 10.1063/1.2963992]

I. INTRODUCTION

Organic photovoltaic devices provide a promising path towards ecologically friendly, low cost energy production. Hence, much effort is spent in increasing the efficiency of such devices in order to make them competitive to their inorganic counterparts. Up to now, small-area organic solar cells (OSCs) are capable of reaching power conversion efficiencies of about 5%,[1,2] while model calculations predict that it is possible to obtain 10%–11%[3,4] within blended single layer structures. On one hand, the material related limitation of open circuit voltage and photocurrent of present-day devices limits the efficiency. This problem is addressed by modifying the active heterojunction either by implementing alternative materials or by influencing the morphology of the donor-acceptor blend.[5–7] On the other hand, a rather high series resistance due to Ohmic losses and suboptimal charge collection efficiency at the electrodes can restrict the fill factor.

Both obstacles mentioned above can be tackled separately by fabricating OSCs in the so-called *p-i-n* architecture.[8] Its concept is shown in Fig. 1. The active area where the incoming light is absorbed and photogenerated excitons are transformed into free charge carriers usually consists of a blend of donor and acceptor type materials. It is embedded between the charge carrier transport layers, which are composed of molecularly doped organic compounds. Doping increases the conductivity and therefore ensures an efficient charge transport and the formation of Ohmic contacts at organic/metal interfaces.[9] In order to obtain efficient devices, the transport layers need to fulfill some criteria such as dopability, thermal and morphological stability, as well as high charge carrier mobility. Energy level alignment relative to the neighboring active layer will lead to an efficient charge extraction. Another preferable material property is transparency, which yields the following advantages: (1) The light intensity reaching the active area is not weakened by parasitical absorption in the transport layers. Excitons are only generated within the active layers. (2) An offset between, e.g., the highest occupied molecular orbital (HOMO) levels of acceptor and electron transport layer (ETL) leads to the existence of an energy barrier at the interface, which inhibits the excitons to diffuse into the doped layers where they would be quenched readily at the dopant molecules. (3) The same energy barrier prevents holes from diffusing into the ETL. It works like a selective membrane, which consequently supports unidirectional transport. (4) As depicted schematically in Fig. 1, the reflection of the incoming light at the metal top contact will lead to the formation of a standing wave. By adjusting the thickness of the transport layers, the active area can be shifted to the maximum of the resulting field distribution. Since doped layers have a sufficiently high conductivity allowing the use of even thick layers

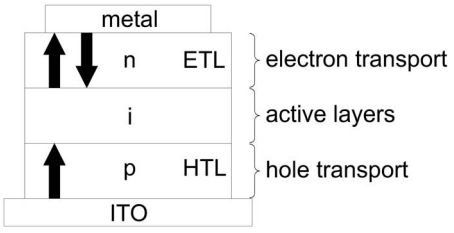

FIG. 1. Schematic structure of an OSC according to the *p-i-n* concept: Light enters the stack through the ITO bottom contact and is reflected at the metal top contact. The maximum of the resulting field distribution can be adjusted to the photovoltaic active layers by means of thickness variation of the transport layers. While the active materials are intrinsic (i) the hole transport layer (HTL) is *p*-doped and the electron transport layer (ETL) is *n*-doped.

[a]Electronic mail: christiane.falkenberg@iapp.de.
[b]Present address: Heliatek GmbH, Liebigstr. 26, D-01187 Dresden, Germany.
[c]Electronic mail: leo@iapp.de.

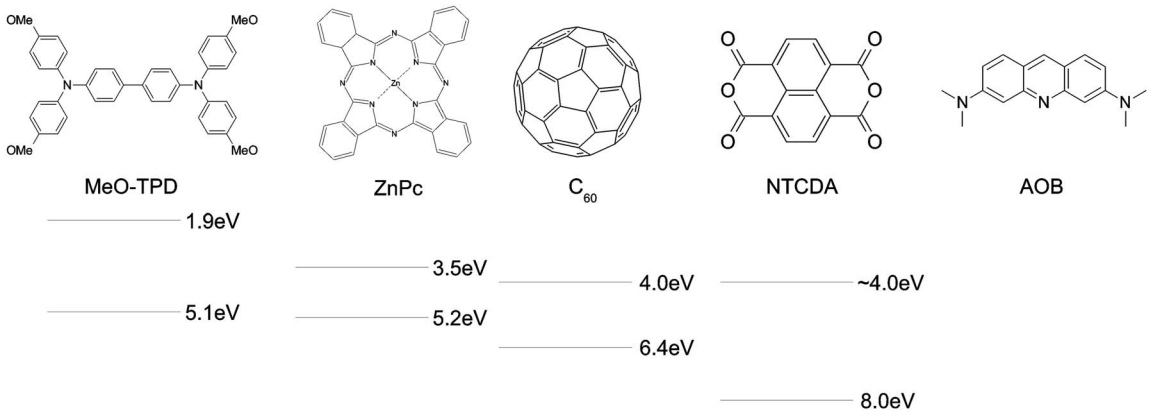

FIG. 2. Molecular structure of the materials used: *N*,*N*,*N*′,*N*′-tetrakis(4-methoxyphenyl)-benzidine (MeO-TPD), zinc-phthalocyanine (ZnPc), C_{60}, 1,4,5,8-naphthalenetetracarboxylic dianhydride (NTCDA), and the molecular dopant acridine orange base (AOB) and their HOMO/LUMO positions[18–20,15].

($\leq$100 nm), the extension of the charge transport layers can be varied without risking considerable Ohmic losses.[8]

Unfortunately, there are up to now only few electron conducting materials known, which meet all desired requirements. As a standard layer sequence for the *n*-side exciton blocking layer (EBL)/metal[10,11] or *n*-C_{60}/metal [12] is currently used, although this approach can still be improved. This paper presents the electron transport material 1,4,5,8-naphthalenetetracarboxylic dianhydride (NTCDA) as a promising substitute for the standard electron transport system. Its applicability as an undoped thick (600 nm–2 μm) charge transport and protection layer in organic photovoltaic devices has been shown previously by Suemori *et al.*[13,14] In contrast, we focus on the implementation of the *p-i-n* concept and thus use comparatively thin layers of *n*-doped NTCDA. Since its lowest unoccupied molecular orbital (LUMO) position of ~4 eV[15] is similar to that of C_{60}, the same molecular dopants can be used for improving the transport properties. Upon doping with acridine orange base (AOB) or the Novaled *n*-dopant NDN1 the conductivity of NTCDA is increased by three to four orders of magnitude compared to the undoped case and reaches $\sigma = 1.2 \times 10^{-4}$ S/cm.[16] In combination with active systems that usually incorporate ZnPc or CuPc as donor materials blended with C_{60} as an acceptor, NTCDA shows a good LUMO level alignment. Hence, electrons are extracted without encountering an energy barrier. However, the most important fact is that in contrast to C_{60} NTCDA is a widegap material and therefore does not absorb in the visible range.

Our work shows that the above stated advantages of wide-bandgap materials can indeed improve the power conversion efficiency.

II. EXPERIMENT

The molecular structures of the organic semiconductors we use for sample preparation are depicted in Fig. 2. Before use, all materials were purified at least twice by vacuum gradient sublimation. *N*,*N*,*N*′,*N*′-tetrakis(4-methoxyphenyl)-benzidine (MeO-TPD) (Sensient, Wolfen, Germany) serves as a matrix material for the hole transport, zinc phthalocyanine (ZnPc) (Alpha Aesar, Karlsruhe, Germany) and C_{60} (Kurchatov Institute, Moscow) are used as active materials. Finally NTCDA (Sigma-Aldrich, St. Louis, USA) is employed as a matrix material for the electron transport with reference to the formerly used acceptor C_{60} as an ETL. At the *p*-side, the Novaled *p*-dopant 2 (NDP2) (Novaled GmbH) is used instead of the comparable material 2,3,5,6-tetrafluoro-7,7,8,8-tetracyanoquinodimethan (F_4-TCNQ) while at the *n*-side either AOB (Sigma-Aldrich) or the comparable Novaled *n*-dopant 1 (NDN1) (Novaled GmbH, Dresden, Germany) is chosen. The use of the Novaled dopants does not cause any significant influence on the device performance, but alleviates materials handling.

All devices are prepared on ITO-coated glass substrates (indium tin oxide from Thin Film Devices Inc., Anaheim, USA, sheet resistance <30 Ω/sq), which were precleaned with organic solvents in an ultrasonic bath. Thermal evaporation is performed at $p < 10^{-6}$ mbar and deposition rates of ~0.5 Å/s in one of the two different UHV systems. Either a multichamber UHV system is used in which the intrinsic layers, all doped layers, as well as the metal layers are deposited in separate chambers without breaking the vacuum. Alternatively, all layers are deposited successively in a single large chamber (K. J. Lesker, Hastings, England). That way, it is possible to fabricate several devices with different structures on the same substrate, ensuring the same preparation conditions, i.e., comparability for the solar cells under consideration. Doping is realized by the coevaporation of matrix and dopant material from different crucibles while the deposition rates are controlled individually by quartz oscillators. Right after processing, all devices are encapsulated. The *J-V*-characteristics are recorded under a simulated AM1.5 illumination provided by a sun simulator SOL 1200 (Hoenle AG, Gräfelfing, Germany). While the current is detected with a Keithley Source Measure Unit (SMU236) the intensity at the sample position is registered with the help of a silicon reference cell (Fraunhofer Institut für Solare Energiesysteme, Freiburg, Germany). A possible mismatch between the simulated and the AM1.5 spectrum or between the spectral responses of the reference cell and the test device is not accounted for. The devices have an average active area of 6.6 mm^2.

For determining the optical density, NTCDA and C_{60} thin films of different thicknesses are deposited onto a quartz

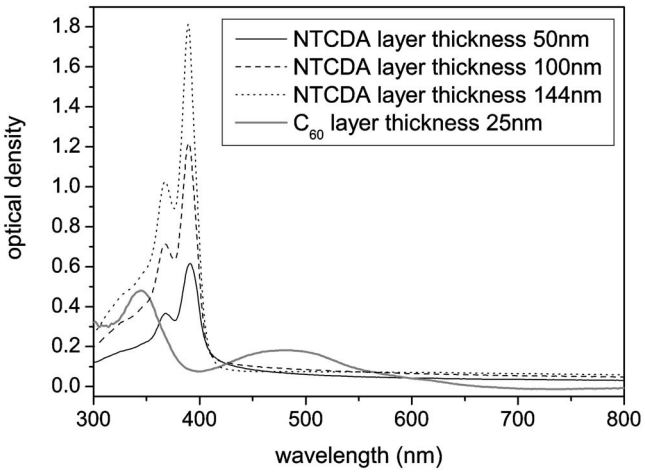

FIG. 3. Optical density of NTCDA thin films with 50 (solid line), 100 (dashed line), and 144 nm (dotted line) thicknesses, respectively, compared with the optical density of a 25 nm thick C_{60} layer (gray line).

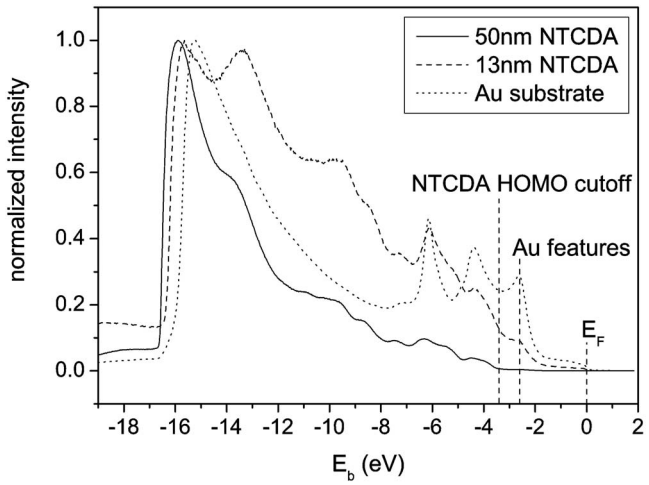

FIG. 4. Normalized UPS spectra of the Au substrate (dotted), 13 nm NTCDA on Au (dashed) and 50 nm NTCDA on Au (solid).

glass substrate. The UV-vis spectra are recorded using a Shimadzu UV/VIS-3100 spectrometer. The measurements are performed in air shortly after sample preparation.

The electronic structure of NTCDA and the interface characteristics between AOB doped NTCDA and aluminum are determined by X-Ray and ultraviolet photoelectron spectroscopy (XPS/UPS) in a separate UHV chamber ($p \leq 10^{-9}$ mbar), which is connected to the preparation chamber. A molybdenum substrate is covered by a clean metal layer, followed by a stepwise deposition of the organic layers. After each step, a UPS measurement using a He I (21.2 eV) discharge lamp and an XPS measurement using the Al K_α radiation (1486.6 eV) is performed. A hemispherical electron spectrometer Phoibos 100 (Specs, Berlin, Germany) is used to record the electronic energy distribution.

III. RESULTS AND DISCUSSION

A. Optical properties

The optical gap of NTCDA was determined from the absorption spectra of NTCDA thin films, which were prepared on a quartz glass. Figure 3 shows the optical density of a 50, a 100, and a 144 nm thick NTCDA layer, respectively. The spectra show a broad absorption band between 300 and 400 nm with local maxima at 390 and 368 nm as well as a shoulder at ~332 nm. As expected, the optical density increases with film thickness. The optical gap E_G^{opt} is derived as follows from the band edge at low energies, which is extrapolated to 406.5 nm:

$$E_G^{\mathrm{opt}} = \frac{hc}{\lambda_{\max}} = \frac{1240.17\ \mathrm{eV\ nm}}{406.5\ \mathrm{nm}} = 3.05\ \mathrm{eV}.$$

As the HOMO/LUMO-gap corresponds to the electronic bandgap, it exceeds the optical gap by the absolute value of the exciton binding energy. Nevertheless, the above shown result proves that NTCDA is indeed a widegap material, which does not absorb in the visible range of the solar spectrum. C_{60} in contrast has a broad absorption peak in the visible range, which is also shown in Fig. 3. Contrary to C_{60}, NTCDA very well fulfills the demands of the *p-i-n* concept on the optical properties of an electron transport material.

B. Photoelectron spectroscopy

The HOMO position of NTCDA was determined by performing UPS measurements of undoped NTCDA, which had been deposited onto a Au substrate. Since gold as a noble metal is not very reactive, the obtained ionization potential (IP) acts as a reference for later results for NTCDA on Al. Figure 4 shows the UPS spectra of the Au substrate as well as the spectra of a 13 and a 50 nm NTCDA layer on top of this substrate. For the thinner organic layers, the features of the Au valence levels and the Au Fermi edge are still visible. This result suggests that a 13 nm thick NTCDA layer is not yet closed. The first and the third peaks cannot be attributed to NTCDA reliably since they have the same absolute positions as the respective gold valence peaks. However, the second gold peak is not located exactly on the second shoulder of the NTCDA spectrum; therefore this shoulder might represent the actual NTCDA HOMO peak. This assumption is confirmed by the 50 nm NTCDA spectrum in which all gold features have vanished and the HOMO cutoff can clearly be assigned to an energy of 3.4 eV below the Fermi edge of the substrate. The IP as derived from the width of the spectrum yields 8.0 eV and agrees well with the value derived by Chan *et al.* in 2006.[15]

All OSCs that are fabricated in *p-i-n* geometry have Al top contacts. Therefore the relative positions of molecular levels across this metal/organic interface are of great interest. By depositing seven layers of organic material successively onto a freshly sputtered Al substrate and measuring the UPS and XPS spectra after each step, the shift of the energy levels is monitored. The XPS data that support the findings of the UPS measurements are not shown here. The interesting regions of the UPS data are shown in Fig. 5. For layers thicker than 1 nm, the Fermi edge of the Al vanishes. Considering that the Fermi edge of the gold substrate is still visible at a coverage of 13 nm NTCDA, one can conclude a different strength of interaction between NTCDA and aluminum leading to an altered growth mode. With increasing layer thick-

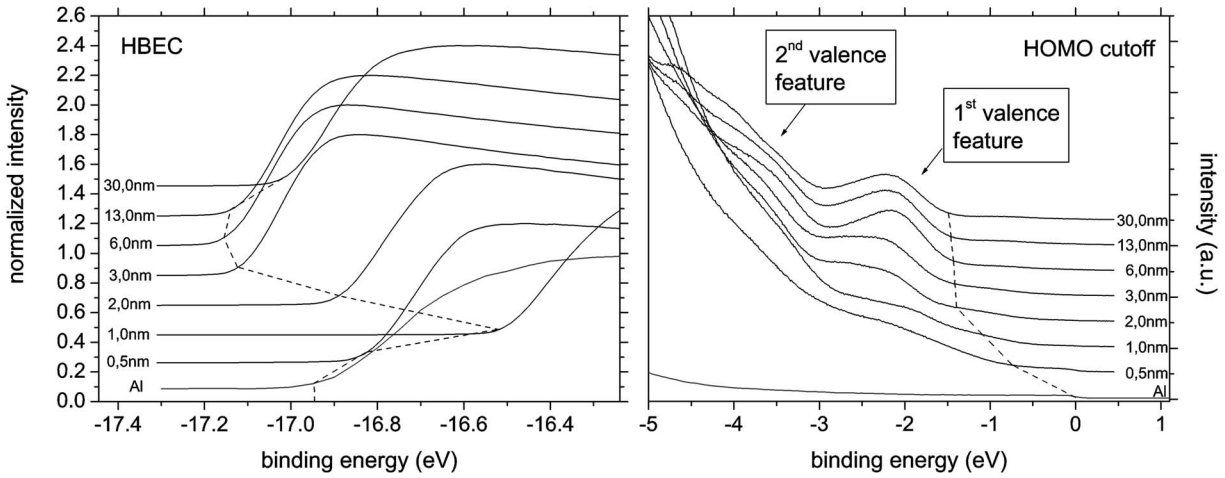

FIG. 5. Magnification of the high binding energy cutoff (HBEC) region and the HOMO region of the UPS spectra of successively grown NTCDA layers on an Al substrate. Curves for different layer thicknesses are plotted with an intensity offset. The layer thickness dependent evolution of the HBEC and the HOMO cutoff is outlined by the dashed curve.

ness, the spectrum as a whole shifts towards higher binding energies, which can be quantified by the shifts of the high binding energy cutoff (HBEC) and the HOMO cutoff. The hole injection barrier is derived as

$$\mathrm{HIB} = E_F - \mathrm{HOMO}_{\mathrm{cutoff}}(30\ \mathrm{nm}) = 0.7\ \mathrm{eV}.$$

The change of the HBEC reveals the interface dipole (ID) between the metal and the organic, which is complete at an NTCDA layer thickness of 1 nm and has a value of 0.46 eV. Further HBEC shifts beyond this thickness are attributed to the doping induced energy level bending, which has a total value of 0.59 eV. Evaluating the width of the spectrum at 30 nm yields the IP of NTCDA as follows:

$$\mathrm{IP}_{\mathrm{NTCDA}} = 21.22\ \mathrm{nm} - |(\mathrm{HOMO} - \mathrm{HBEC})_{30\ \mathrm{nm}}|,$$

$$\mathrm{IP}_{\mathrm{NTCDA}} = 5.68\ \mathrm{eV}.$$

A similar value has been determined by Suemori *et al.* with 5.5 eV.[13] This result not only contradicts the value obtained for NTCDA on Au, but also conflicts with the material properties reported above. Considering an optical gap of 3.05 eV, the LUMO would be at 2.5–2.0 eV (depending on the respective exciton binding energy). If this were true, the material would neither be dopable with AOB nor with NDN1. Energy level alignment with the C_{60} LUMO would not be given and therefore it would not be possible to fabricate working OSCs in *p-i-n* geometry as shown in Sec. III C. Therefore, we assume the first HOMO peak to be a defect state within the energy gap while the second peak relative to the Fermi edge is assigned to the actual HOMO. Due to the superposition of this peak with the defect state, its cutoff can only be estimated to 2.9 eV, yielding an IP of 6.97 eV, which is about 1 eV below the formerly stated IP of 8.0 eV. Up to now, one can only speculate about the origin of the defect state. Assigning it to a feature of the underlying Al substrate is not an option since there are no Al valence peaks at this energy position. According to Maruyama *et al.*,[17] who have observed a similar gap state for NTCDA on indium, a chemical reaction with metal atoms diffusing into the organic layers could be responsible for the formation of an additional state. Alternatively, a reaction with the dopant AOB as a result of the electron transfer cannot be excluded as an explanation. It is, however, questionable if the low dopant concentration within the matrix material suffices for the formation of a pronounced defect state.

C. Organic solar cells containing NTCDA as ETL

Two OSCs with the structure ITO/NDP2(1 nm)/MeO-TPD:NDP2(30 nm,30:1)/C_{60}:ZnPc(37.7 nm,1:1)/*i*-C_{60}(26 nm)/ETL:NDN1(~40 nm)/Al were prepared on the same substrate at the same time, i.e., under the same conditions. The ETL matrix material is either 39 nm of C_{60} (doping ratio 65:1) in cell *A* or 40 nm of NTCDA (doping ratio 50:1) in cell *B*. Thus it is possible to directly compare the device characteristics depending on the choice of the matrix material for electron transport. The active layers consist of a bulk C_{60}:ZnPc heterojunction and an additional 26 nm

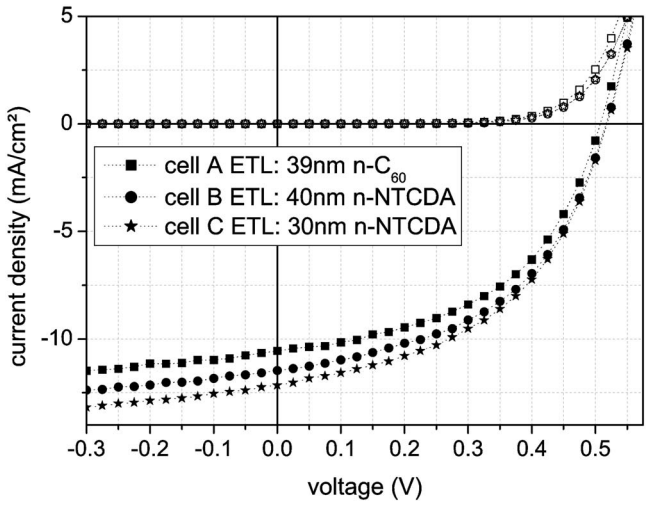

FIG. 6. *J-V*-characteristics of three solar cells either comprising NDN1-doped C_{60} (39 nm, 65:1) in cell *A* or NDN1-doped NTCDA in cell *B* (40nm, 50:1), and cell *C* (30 nm, 50:1) as an electron transport material. The open points correspond to the *J-V*-characteristics measured in the dark.

TABLE I. Short circuit current density, open circuit voltage, fill factor, and efficiency of the reported solar cells *A* (comprising C_{60} as an ETL), *B* (comprising NTCDA as an ETL), and the optimized cell structure *C*. The current densities are corrected for 100 mW/cm^2 intensity.

Cell	ETL	I_{sun} (mW/cm^2)	J_{sc} (mA/cm^2)	V_{oc} (V)	FF (%)	η_{PCE} (%)
A	39 nm *n*-C_{60}	107.3	9.83	0.51	49.4	2.47
B	40 nm *n*-NTCDA	105.8	10.84	0.52	48.7	2.73
C	30 nm *n*	106.5	11.41	0.52	47.8	2.83

thick intrinsic C_{60} layer. Figure 6 shows the *J-V*-characteristics of both cells while the resulting parameters are given in Table I. All current densities are corrected for 100 mW/cm^2 intensity. The solar cell *B* containing NTCDA clearly shows a better cell performance: compared with cell *A*, the short circuit current density is enhanced to $J_{sc,B}=10.84$ mA/cm^2 from $J_{sc,A}=9.83$ mA/cm^2, i.e., by ~10% while the open circuit voltage increases from $U_{oc,A}=0.51$ V to $U_{oc,B}=0.52$ V. The efficiency is also increased by ~10% from $\eta_{PCE,A}=2.47\%$ to $\eta_{PCE,B}=2.73\%$. The fill factor, however, does not follow this tendency since it is slightly decreased for the NTCDA device.

According to the *p-i-n* concept, there are two possible explanations for the behavior of the current densities. If the ETL consists of a light absorbing material such as C_{60}, the overall photon density in the active layers is decreased. Hence, the number of generated excitons is smaller in devices with parasitically absorbing transport layers. Second, there is no energy barrier between the HOMO and LUMO states of doped and intrinsic C_{60}. Therefore excitons are able to pass this interface easily and can quench at the dopant molecules or the metal contact. Consequently, the number of excitons that reach the donor/acceptor heterojunction and that are separated into free charge carriers is much higher in NTCDA solar cells than in C_{60} solar cells.

In order to find an optimized cell structure, the *i*-C_{60} layer thickness as well as the *n*-NTCDA layer thickness were varied while the rest of the stack was kept unchanged. As a result the structure ITO/NDP2(1 nm)/*p*-MeO-TPD (30 nm)/ZnPc:C_{60}(37.7 nm,1:1)/*i*-C_{60}(26 nm)/NTCDA:NDN1(30 nm,50:1)/Al (cell *C*) turned out to have the highest efficiency with $\eta_{PCE}=2.83\%$. The *J-V*-curve is shown in Fig. 6 and the cell parameters are listed in Table I. We explain this behavior in terms of the modified *p-i-n* geometry, which changes the distribution of the optical field inside the layer structure. For cell *C*, the active area is positioned in the maximum of the intensity, which correlates with enhanced exciton generation.

All attempts to fabricate OSCs with an inverted cell structure, so-called *n-i-p* cells, resulted in short circuits since the morphology of NTCDA influences the morphology of all following layers markedly.[16] The same effect prevented the production of tandem solar cells containing thick layers of *n*-doped NTCDA in the recombination zone.

IV. CONCLUSION

It was demonstrated that NTCDA is a useful electron transport material, which is able to replace the standard system consisting of either *n*-doped C_{60} or a thick layer of intrinsic C_{60} with an EBL. The advantageous positions of the HOMO and LUMO levels of NTCDA guarantee a loss free charge extraction from the active layers and exciton blocking simultaneously. However, the morphology represents an important drawback making it impossible to implement device architectures different from the *p-i-n* structure. Nevertheless, it was possible to fabricate efficient OSCs incorporating *n*-NTCDA as an ETL, which were superior to identical devices incorporating *n*-C_{60}. The best efficiency reached was $\eta_{PCE}=2.83\%$.

The results of this work underline the advantages of transparent charge carrier transport materials. In order to further improve the functionality of organic photovoltaic devices, it will be necessary to continue the search for functionalized materials. Especially an accurate adjustment of HOMO and LUMO levels relative to the respective active material plays a crucial role. As the examination of NTCDA shows the thin-film morphology, i.e., the glass transition temperature, is also an important criterion. However, the formation of smooth amorphous layers upon vacuum deposition should not take place at the expense of the charge carrier mobility. Gaining control over those material properties by means of a selective synthesis of molecular materials for OSC production will remain a challenge.

ACKNOWLEDGMENTS

We would like to thank the Bundesministerium für Bildung und Forschung (BMBF) for funding this work within the scope of the Innoprofile project 03IP602.

[1] J. G. Xue, B. P. Rand, S. Uchida, and S. R. Forrest, J. Appl. Phys. **98**, 124903 (2005).
[2] W. L. Ma, C. Y. Yang, X. Gong, K. Lee, and A. J. Heeger, Adv. Funct. Mater. **15**, 1617 (2005).
[3] L. J. A. Koster, V. D. Mihailetchi, and P. W. M. Blom, Appl. Phys. Lett. **88**, 093511 (2006).
[4] M. C. Scharber, D. Wuhlbacher, M. Koppe, P. Denk, C. Waldauf, A. J. Heeger, and C. L. Brabec, Adv. Mater. (Weinheim, Ger.) **18**, 789 (2006).
[5] K. Schulze, C. Uhrich, R. Schueppel, K. Leo, M. Pfeiffer, E. Brier, E. Reinold, and P. Bäuerle, Adv. Mater. (Weinheim, Ger.) **18**, 2872 (2006).
[6] Z. R. Hong, B. Maennig, R. Lessmann, M. Pfeiffer, K. Leo, and P. Simon, Appl. Phys. Lett. **90**, 203505 (2007).
[7] S. M. Schultes, P. Sullivan, S. Heutz, B. M. Sanderson, and T. S. Jones, Mater. Sci. Eng., C **25**, 858 (2005).
[8] B. Maennig, J. Drechsel, D. Gebeyehu, P. Simon, F. Kozlowski, A. Werner, F. Li, S. Grundmann, S. Sonntag, M. Koch, K. Leo, M. Pfeiffer, H. Hoppe, D. Meissner, N. S. Sariciftci, I. Riedel, V. Dyakonov, and J. Parisi, Appl. Phys. A: Mater. Sci. Process. **79**, 1 (2004).
[9] W. Y. Gao and A. Kahn, Org. Electron. **3**, 53 (2002).
[10] M. Y. Chan, C. S. Lee, S. L. Lai, M. K. Fung, F. L. Wong, H. Y. Sun, K. M. Lau, and S. T. Lee, J. Appl. Phys. **100**, 094506 (2006).
[11] P. Peumans, V. Bulovic, and S. R. Forrest, Appl. Phys. Lett. **76**, 2650

(2000).
[12]J. Drechsel, B. Maennig, F. Kozlowski, D. Gebeyehu, A. Werner, M. Koch, K. Leo, and M. Pfeiffer, Thin Solid Films **451**, 515 (2004).
[13]K. Suemori, T. Miyata, M. Yokoyama, and M. Hiramoto, Appl. Phys. Lett. **86**, 063509 (2005).
[14]K. Suemori, Y. Matsumura, M. Yokoyama, and M. Hiramoto, Jpn. J. Appl. Phys., Part 2, **45**, L472 (2006).
[15]C. K. Chan, E. G. Kim, J. L. Brédas, and A. Kahn, Adv. Funct. Mater. **16**, 831 (2006).
[16]C. Falkenberg, C. Uhrich, B. Maennig, M. K. Riede, and K. Leo, Proc. SPIE **6999**, 69990S (2008).
[17]T. Maruyama, N. Sugawara, A. Hirasawa, and K. Akimoto, Surf. Sci. **493**, 697 (2001).
[18]G. F. He, M. Pfeiffer, K. Leo, M. Hofmann, J. Birnstock, R. Pudzich, and J. Salbeck, Appl. Phys. Lett. **85**, 3911 (2004).
[19]W. Y. Gao and A. Kahn, Appl. Phys. Lett. **82**, 4815 (2003).
[20]O. V. Molodtsova and M. Knupfer, J. Appl. Phys. **99**, 053704 (2006).